

Non-Hermitian Skin Effect Edge

Qi-Bo Zeng*

Department of Physics, Capital Normal University, Beijing 100048, China

Non-Hermitian skin effect (NHSE) is a unique phenomenon studied intensively in non-Hermitian systems during the past few years. In this work, we show that NHSE can be energy dependent by introducing long-range nonreciprocal hopping into the one-dimensional lattices. The direction of NHSE reverses as the eigenenergy of the system under open boundary conditions (OBCs) sweeps across some critical energies. To characterize such a phenomenon, we introduce the concept of non-Hermitian skin effect edges, which separate the eigenstates localized at opposite ends of the lattice in the OBC spectrum. We find the skin effect edges are determined by the self-intersections in the spectrum under periodic boundary conditions (PBCs), which are topological as the winding number of the PBC spectrum changes sign when crossing them. Moreover, the NHSE edges will disappear when the self-intersections merge into a single point by tuning the system parameters. Our work reveals the intricate interplay between NHSE and long-range hopping in non-Hermitian systems.

Non-Hermitian physics has attracted intensive attention recently [1–5]. It is known that non-Hermitian Hamiltonians can describe open systems effectively and have been exploited to study the properties of various classical [6–16] as well as quantum systems [17–26]. Though the energy spectra of non-Hermitian Hamiltonians are general complex, the discovery of real spectra in systems with \mathcal{PT} -symmetry [27–29] or pseudo-Hermiticity [30–35] has intrigued a persistent exploration of non-Hermitian systems in the past two decades.

Another unique phenomenon in non-Hermitian systems is the non-Hermitian skin effect (NHSE), where a macroscopic number of eigenstates accumulate at a boundary of the system [36, 37]. Recently, a large volume of research has been dedicated to investigating the exotic properties due to NHSE [38–49]. For instance, it has been shown that NHSE can modify the band topology significantly and break down the conventional principle of bulk-boundary correspondence in topological phases [36, 37, 50–58]. In addition, the NHSE also influences the phenomenon of Anderson localization significantly [62–68]. The eigenenergy spectra of the extended and localized states exhibit different topology under periodic boundary conditions (PBCs) [66]. In addition, the NHSE can induce mobility edges in the disordered non-Hermitian system, which separates the localized and extended states in the spectrum [64]. It is interesting to ask whether the NHSE will also show similar energy-dependent features. Since most studies on NHSE to date have focused on systems with only nearest-neighbor hopping and the NHSE is energy independent, we need to check how long-range hopping influences the behavior of NHSE.

To answer the above questions, we study the one-dimensional (1D) lattices with long-range nonreciprocal hopping in this paper. We show that the NHSE can be energy dependent in that some eigenstates are localized at the left end of the lattice while the others localized at the right end under open boundary conditions (OBCs). The direction of the NHSE reverses as the en-

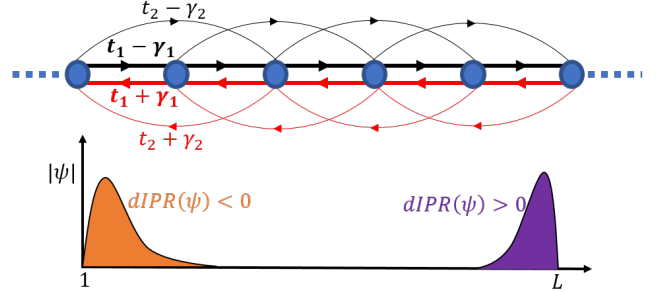


FIG. 1. (Color online) Schematic of 1D lattice with non-reciprocal hoppings between the nearest- and next-nearest-neighbor sites, which are represented by $(t_1 \pm \gamma_1)$ and $(t_2 \pm \gamma_2)$, respectively. The lower panel shows the distribution of the eigenstates with positive and negative dIPR values.

ergy sweeps across the critical energies. We thus define the concept of non-Hermitian skin effect edge, which separates the states localized at opposite ends of the 1D lattices in the energy spectrum. More interestingly, we find that the skin effect edges are determined by the self-intersections in the spectrum under PBCs. The winding number of the PBC spectrum changes sign by crossing the self-intersecting points, implying the topological feature of the skin effect edge. The self-intersections will merge into a single point as we tune the system parameters, leading to the disappearance of NHSE edges. Our work unveils the exotic properties of NHSE in the non-Hermitian systems with long-range hopping.

Model.—We introduce the general 1D lattices with long-range nonreciprocal hopping described by the following model Hamiltonian

$$H = \sum_{j=1}^{L-r_d} \sum_{s=1}^{r_d} \left[(t_s - \gamma_s) c_{j+s}^\dagger c_j + (t_s + \gamma_s) c_j^\dagger c_{j+s} \right], \quad (1)$$

where c_j (c_j^\dagger) is the annihilation (creation) operator of spinless fermions at the j th site. The forward and backward hopping amplitudes are $(t_s - \gamma_s)$ and $(t_s + \gamma_s)$ with t_s and γ_s being real numbers. L is the lattice

size. r_d is a positive integer and is the cutting range of the hopping, which means that the hopping extends to the nearest r_d sites. If $r_d = 1$, the system reduces to the Hatano-Nelson (HN) model with nearest-neighbor (NN) hopping. If $r_d = 2$, the Hamiltonian includes the next-nearest-neighbor (NNN) hopping and is called the $t_1 - t_2$ model in the Hermitian case when introduced quasiperiodic onsite potentials, which is useful in studying the mobility edge and localization properties in 1D lattices [69]. Throughout this paper, we will take $t_1 = 1$ as the energy unit.

With the presence of nonreciprocity in the hopping terms, there will be NHSE in the system and the eigenstates will become localized at the end of the 1D lattice. To characterize the localization of the states we may use the inverse participation ratio (IPR), which is defined as $\text{IPR} = \sum_{j=1}^L |\Psi_{n,j}|^4 / (\langle \Psi_n | \Psi_n \rangle)^2$ and has been extensively used in describing Anderson localization phenomenon. Here Ψ_n is the right eigenstate with component $\Psi_{n,j}$ and satisfies the Schrödinger equation $H\Psi_n = E_n\Psi_n$, with E_n being the n th eigenenergy. The IPR is close to 0 for the extended state but of the order $O(1)$ for the localized state. To distinguish the states localized at different ends of the 1D lattice due to NHSE, we introduce the directional IPR (dIPR) as [49]

$$\text{dIPR}(\Psi_n) = \mathcal{P}(\Psi_n) \sum_{j=1}^L \frac{|\Psi_{n,j}|^4}{(\langle \Psi_n | \Psi_n \rangle)^2}, \quad (2)$$

with $\mathcal{P}(\Psi_n) = \text{sgn} \left[\sum_{j=1}^L (j - \frac{L}{2} - \delta) |\Psi_{n,j}| \right]$. Here $\delta \in (0, 0.5)$ is a constant. $\text{sgn}(x)$ takes the sign of the argument, which is positive (negative) for $x > 0$ ($x < 0$). The dIPR is positive when Ψ_n is localized at the right end but is negative when Ψ_n is localized at the left end. If $\text{dIPR} \rightarrow 0$, then the state is extended.

Non-Hermitian skin effect edge.—We mainly consider the 1D lattices with NNN hopping, i.e., we set $r_d = 2$ in Eq. (1) and obtain

$$H_2 = \sum_{j=1}^{L-2} \left[(t_1 - \gamma_1) c_{j+1}^\dagger c_j + (t_2 - \gamma_2) c_{j+2}^\dagger c_j + (t_1 + \gamma_1) c_j^\dagger c_{j+1} + (t_2 + \gamma_2) c_j^\dagger c_{j+2} \right]. \quad (3)$$

By transferring H_2 into the momentum space with $k \in [-\pi, \pi)$, we get the PBC spectrum as

$$E_2(k) = 2[t_1 \cos(k) + t_2 \cos(2k)] + 2i[\gamma_1 \sin(k) + \gamma_2 \sin(2k)]. \quad (4)$$

To illustrate the effect of the NNN hopping on the NHSE, we first set $\gamma_1 = t_2 = 0$ and check the properties of the following simplified Hamiltonian

$$H'_2 = \sum_{j=1}^{L-2} \left[t_1 c_{j+1}^\dagger c_j + t_1 c_j^\dagger c_{j+1} - \gamma_2 c_{j+2}^\dagger c_j + \gamma_2 c_j^\dagger c_{j+2} \right]. \quad (5)$$

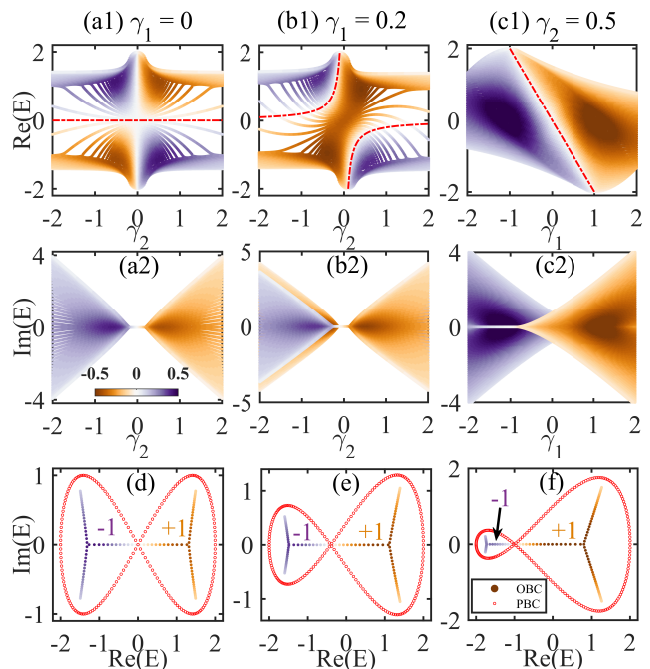


FIG. 2. (Color online) (a1)-(c1) Real and (a2)-(c2) imaginary parts of the OBC eigenenergy spectra of H_2 with $t_2 = 0$ as a function of γ_2 or γ_1 . The colorbar indicates the dIPR value of the eigenstate. The red dot-dashed lines are the non-Hermitian skin effect edges. The lowest panel shows the OBC (solid dots) and PBC (red empty dots) spectra of the systems with $\gamma_2 = 0.5$ and $\gamma_1 = 0.0, 0.2$, and 0.5 in (d)-(f), respectively. The numbers ± 1 are the winding numbers for the PBC spectra. The lattice size is $L = 120$.

Due to the opposite signs of the NNN forward and backward hopping terms in the system, the skin effect shows up even though the strength are both $|\gamma_2|$, as shown in Fig. 2(a). More interestingly, when $\gamma_2 > 0$ (or $\gamma_2 < 0$), half of the eigenstates with $\text{Re}(E) < 0$ [or $\text{Re}(E) > 0$] are localized at the right end of the lattice; while the other half with $\text{Re}(E) > 0$ [or $\text{Re}(E) < 0$] are localized at the left end. This is totally different from the NHSE shown in systems with NN asymmetric hopping, where all the eigenstates localize at the same end. Here the skin effect is energy dependent and the line $\text{Re}(E) = 0$ separates the states localized at opposite ends. The direction of NHSE reverses when the energy sweeps across the line. Analogous to the definition of mobility edge, which separates extended states from localized states in disordered systems, here we define non-Hermitian skin effect edge as the energy separating the states localized at different ends of the 1D lattice. So, for the simple model in Eq. (5), the skin effect edge is the zero energy. The eigenstate corresponding to the critical energy is extended. If we have $\gamma_1 \neq 0$, the skin effect edge will deviate from zero energy, as shown in Fig. 2(b). The red dot-dashed lines in the real part are the NHSE edges described by the equation $\text{Re}(E) = -\frac{\gamma_1}{\gamma_2} t_1$. If we plot the eigenenergy

as a function of γ_2 , the skin effect edge is a straight line, see Fig. 2(c). We find that for the systems with $t_2 = 0$, the skin effect edge is always real.

It is known that NHSE is closely connected with the point gap in the PBC spectrum [71, 72]. For the energy-dependent NHSE we study here, we can also expect the existence of point gaps. In Fig. 2(d)-2(f), we present the OBC (solid dots) as well as PBC (red empty dots) spectra for systems with $t_1 = 1$, $t_2 = 0$, $\gamma_2 = 0.5$, and different γ_1 values. The PBC spectrum is inseparable and intersects with itself. The loops in the spectrum are characterized by the winding number defined as

$$W = \frac{1}{2\pi i} \int_{-\pi}^{\pi} dk \partial_k \arg [E(k) - E_B], \quad (6)$$

where E_B is the base energy. We find that W has opposite signs for the loops enclosing states localized at the opposite ends. For the loop enclosing the states localized at the right (left) end, we have $W = -1$ ($W = +1$). The self-intersecting point of the PBC spectrum is the critical energy that separates the states localized at opposite ends of the system under OBC. The winding number changes sign abruptly as E_B crosses the critical energy. So the NHSE edge in the energy spectrum is topological. By calculating the self-intersections E_2^{SI} in the PBC spectrum, we can obtain the critical energies and thus determine the skin effect edges. To do this, suppose that we have $k_1, k_2 \in [-\pi, \pi)$ and $k_1 \neq k_2$, such that $E_2(k_1) = E_2(k_2)$ with $E(k)$ given in Eq. (4)). For the systems with $t_2 = 0$, the solution to this equation gives us the NHSE edge as (see supplementary [70])

$$\text{Re}(E_2^{SI}) = -\frac{\gamma_1}{\gamma_2} t_1; \quad \text{Im}(E_2^{SI}) = 0, \quad (7)$$

with the restriction $\left| \frac{\gamma_1}{2\gamma_2} \right| \leq 1$, which is consistent with the numerical results shown in Fig. 2.

Now we turn on the NNN hopping t_2 and check how the skin effect edge will change. In Fig. 3(a) and 3(b), we present the real and imaginary parts of the eigenenergy of the system with $t_1 = t_2 = 1$ and $\gamma_2 = 0.5$ as a function of γ_1 . We find that different from the situation with $t_2 = 0$, where the skin effect edge is purely real, the skin effect edge here can be complex. There are three NHSE edges in the spectrum. One of them is real, as indicated by the red dot-dashed line in Fig. 3(a). The other two are complex conjugated, as shown by the black-solid lines in Fig. 3(a) and 3(b). To further illustrate the distinctive features of the energy spectra, we plot the OBC (solid dots) and PBC (red-empty dots) eigenenergy under different γ_1 values on the complex plane, as shown in Fig. 3(c)-3(f). When $\gamma_1 < -0.5$, we can see that there are several loops in the PBC spectrum, which enclose the OBC spectrum with states localized at the different ends of the system. The corresponding winding numbers are $+1$ and -1 , respectively. We can determine the NHSE

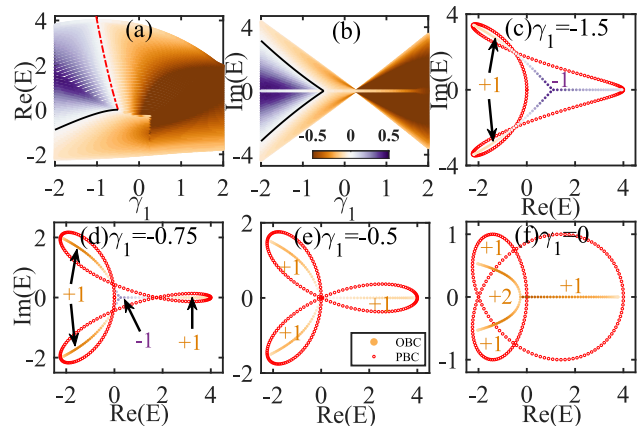


FIG. 3. (Color online) (a) and (b) show the real and imaginary parts of the OBC eigenenergy spectra of H_2 with $t_2 = 1$ as a function of γ_1 . (c)-(f) are the OBC (solid dots) and PBC (red empty dots) spectra with γ_1 varying from -1.5 to 0 . The red dot-dashed lines and black-solid lines are the skin effect edges determined by Eq. (8) and Eq. (9). The numbers indicate the winding numbers of the loops. Here we set $\gamma_2 = 0.5$ and the lattice size $L = 120$.

edge by calculating the self-intersections E_2^{SI} of the PBC spectrum, which gives us the following three analytical expressions (see details in SM [70]):

$$\text{Re}(E_2^{SI1}) = -\frac{\gamma_1}{\gamma_2} t_1 + \left(\frac{\gamma_1^2}{\gamma_2^2} - 2 \right) t_2; \quad \text{Im}(E_2^{SI1}) = 0. \quad (8)$$

$$\begin{aligned} \text{Re}(E_2^{SI2}) = \text{Re}(E_2^{SI3}) &= -\frac{t_1^2}{2t_2} + \frac{t_1\gamma_1}{2\gamma_2} - \frac{2t_2^2\gamma_1}{t_1\gamma_2 - t_2\gamma_1}; \\ \text{Im}(E_2^{SI2}) &= a \left[\frac{\gamma_1}{2t_2\gamma_2} - \left(\frac{t_1}{2t_2^2} - \frac{2\gamma_2}{t_1\gamma_2 - t_2\gamma_1} \right) \right], \\ \text{Im}(E_2^{SI3}) &= a \left[-\frac{\gamma_1}{2t_2\gamma_2} + \left(\frac{t_1}{2t_2^2} - \frac{2\gamma_2}{t_1\gamma_2 - t_2\gamma_1} \right) \right], \end{aligned} \quad (9)$$

where $a = \sqrt{t_1^2\gamma_2^2 - 2t_1t_2\gamma_1\gamma_2}$. These critical energies are exactly the skin effect edges observed in the OBC spectra.

By tuning the system parameters, the self-intersections in the PBC spectrum will merge into one point. The critical parameters for this situation happening are obtained by solving the following equation:

$$E_2^{SI1} = E_2^{SI2} = E_2^{SI3}. \quad (10)$$

For instance, in the system with $t_1 = t_2 = 1$, we find that when $\gamma_1 = -\gamma_2$, the critical lines in the OBC spectrum intersect with each other, leading to the disappearance of the NHSE edges at the intersecting point (see SM for the computation). The loops in the corresponding PBC spectrum are merged at zero energy and form a trefoil, see Fig. 3(e). The winding numbers for the three loops

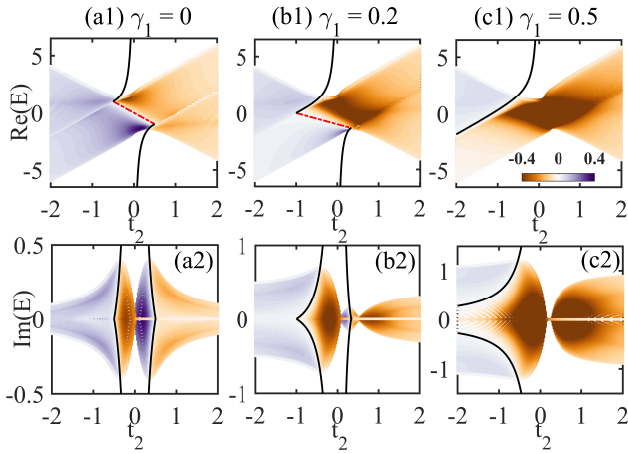


FIG. 4. (Color online) Real and imaginary parts of the OBC eigenenergy of H_2 with $t_1 = 1$ and $\gamma_2 = 0.2$ as a function of t_2 when (a) $\gamma_1 = 0$, (b) $\gamma_1 = 0.2$, and (c) $\gamma_1 = 0.5$. The colorbar indicates the dIPR value of the eigenstates. The red dotted lines and black solid lines are the skin effect edges in Eq. (8) and Eq. (9). The lattice size is $L = 120$.

are $+1$, which indicates that the eigenstates under OBC are all localized at the left end of the lattice. If γ_1 further increases, there will be regions characterized by $W = +2$ in the PBC spectrum, as shown in Fig. 3(f). However, the skin effect edges no longer exist. So, by varying parameters of the long-range system, we can tune the skin effect edge in the OBC spectrum and obtain various spectral topologies in the PBC spectra.

In Fig. 4, we further show the OBC spectra of the system as a function of t_2 . The NHSE edges indicated by the lines are determined by Eq. (8) and 9, respectively. As t_2 varies, these critical lines intersect each other, and the NHSE edges disappear. This corresponds to the merging point obtained by solving Eq. (10). Notice that the real-valued edge (i.e., the red dot-dashed line) in Eq. (8) is restricted in the region $\left| \frac{\gamma_1}{2\gamma_2} \right| \leq 1$ [70]. So if γ_1 becomes too stronger, this NHSE edge will also disappear, as shown in Fig. 4(c).

Skin effect edge in systems with longer-range hopping.—The existence of skin effect edge is not limited to the model with NNN hopping. For systems with even longer range hopping, the NHSE edge still exists. For instance, we can check the system with hopping up to the third or fourth nearest-neighboring sites. The corresponding Hamiltonians are obtained by setting $r_d = 3$ and 4 in Eq. (1). For simplicity, we consider the systems described by H'_3 and H'_4 , which are obtained by replacing γ_2 with γ_3 or γ_4 in Eq. (5), see Refs. [70] and [73].

In Fig. 5, we present the energy spectra of H'_3 and H'_4 as a function of γ_3 and γ_4 . We can see that the real parts of the spectra are divided into several regions according to the positive or negative dIPR values of the eigenstates, while the imaginary parts are not. So there

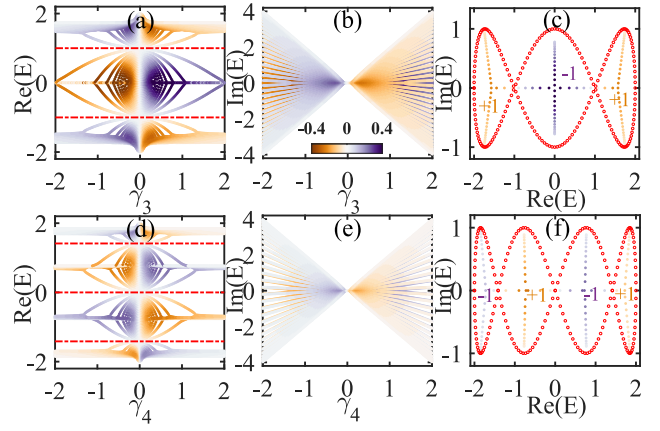


FIG. 5. (Color online) The OBC eigenenergy spectra for H'_3 and H'_4 as a function of the long-range nonreciprocal hopping γ_3 in (a) and (b), or γ_4 in (d) and (e). The red dot-dashed lines are the NHSE edges. (c) and (f) show the PBC (red empty dots) and OBC (solid dots) spectra when $\gamma_3, \gamma_4 = 0.5$, respectively. ± 1 are the winding numbers of the PBC spectra. Here the lattice size is $L = 120$.

are NHSE edges in these systems and the critical energies are real. In Fig. 5(c) and (f), we show the OBC (solid dots) and PBC (red empty dots) spectra for systems with both γ_3 and γ_4 being 0.5 in the complex energy plane. The PBC spectrum forms loops that are characterized by $+1$ (-1) when the enclosed OBC eigenstates localized at the left (right) end of the lattice. The edges thus are topological as the winding number changes suddenly by crossing them. Again we can determine the NHSE edges by calculating the self-intersections in the PBC spectrum, which gives us two self-intersecting points for H'_3 [70]: $E_3^{SI1} = -E_3^{SI2} = t_1$; and three self-intersecting points for H'_4 : $E_4^{SI1} = 0$, $E_4^{SI2} = -E_4^{SI3} = \sqrt{2}t_1$. These are the NHSE edges indicated by the red dot-dashed lines in Fig. 5(a) and 5(d).

In summary, we introduce the concept of non-Hermitian skin effect edge in the 1D systems with long-range nonreciprocal hopping. The NHSE is energy-dependent and the edge separates the eigenstates under OBC localized at opposite ends of the system. The direction of the skin effect reverses as the energy moving across the edge. We also find that the skin effect edges are determined by the self-intersections in the PBC spectrum and are topological as the winding numbers of the PBC spectrum changes sign when crossing the critical points. Our work unveils the exotic properties of the non-Hermitian systems with long-range nonreciprocal hopping.

Acknowledgments: This work is supported by NSFC (Grant No.12204326), R&D Program of Beijing Municipal Education Commission (No. KM202210028017) and Open Research Fund Program of the State Key Laboratory of Low-Dimensional Quantum Physics (No. KF202109).

-
- * zengqibo@cnu.edu.cn
- [1] H. Cao and J. Wiersig, *Rev. Mod. Phys.* **87**, 61 (2015).
 - [2] V. V. Konotop, J. Yang, and D. A. Zezyulin, *Rev. Mod. Phys.* **88**, 035002 (2016).
 - [3] R. El-Ganainy, K. G. Makris, M. Khajavikhan, Z. H. Musslimani, S. Rotter, and D. N. Christodoulides, *Nat. Phys.* **14**, 11 (2018).
 - [4] Y. Ashida, Z. Gong, and M. Ueda, *Advances in Physics* **69**, 3 (2020).
 - [5] E. J. Bergholtz, J. C. Budich, and F. K. Kunst, *Rev. Mod. Phys.* **93**, 015005 (2021).
 - [6] K. G. Makris, R. El-Ganainy, D. N. Christodoulides, and Z. H. Musslimani, *Phys. Rev. Lett.* **100**, 103904 (2008).
 - [7] S. Klaiman, U. Günther, and N. Moiseyev, *Phys. Rev. Lett.* **101**, 080402 (2008).
 - [8] A. Guo, G. J. Salamo, D. Duchesne, R. Morandotti, M. VolatierRavat, V. Aimez, G. A. Siviloglou, and D. N. Christodoulides, *Phys. Rev. Lett.* **103**, 093902 (2009).
 - [9] C. E. Rüter, K. G. Makris, R. El-Ganainy, D. N. Christodoulides, M. Segev, and D. Kip, *Nat. Phys.* **6**, 192 (2010).
 - [10] Z. Lin, H. Ramezani, T. Eichelkraut, T. Kottos, H. Cao, and D. N. Christodoulides, *Phys. Rev. Lett.* **106**, 213901 (2011).
 - [11] A. Regensburger, C. Bersch, M.-A. Miri, G. Onishchukov, D. N. Christodoulides, and U. Peschel, *Nature (London)* **488**, 167 (2012).
 - [12] L. Feng, Y.-L. Xu, W. S. Fegadolli, M.-H. Lu, J. E. B. Oliveira, V. R. Almeida, Y.-F. Chen, and A. Scherer, *Nat. Mater.* **12**, 108 (2013).
 - [13] B. Peng, S. K. Özdemir, F. Lei, F. Monifi, M. Gianfreda, G. L. Long, S. Fan, F. Nori, C. M. Bender, and L. Yang, *Nat. Phys.* **10**, 394 (2014).
 - [14] J. Wiersig, *Phys. Rev. Lett.* **112**, 203901 (2014).
 - [15] H. Hodaei, A. U. Hassan, S. Wittek, H. Garcia-Gracia, R. El-Ganainy, D. N. Christodoulides, and M. Khajavikhan, *Nature (London)* **548**, 187 (2017).
 - [16] W. Chen, S. K. Özdemir, G. Zhao, J. Wiersig, and L. Yang, *Nature (London)* **548**, 192 (2017).
 - [17] D. C. Brody and E.-M. Graefe, *Phys. Rev. Lett.* **109**, 230405 (2012).
 - [18] T. E. Lee and C.-K. Chan, *Phys. Rev. X* **4**, 041001 (2014).
 - [19] J. Li, A. K. Harter, J. Liu, L. de Melo, Y. N. Joglekar, and L. Luo, *Nat. Commun.* **10**, 855 (2019).
 - [20] K. Kawabata, Y. Ashida, and M. Ueda, *Phys. Rev. Lett.* **119**, 190401 (2017).
 - [21] R. Hamazaki, K. Kawabata, and M. Ueda, *Phys. Rev. Lett.* **123**, 090603 (2019).
 - [22] L. Xiao, K. Wang, X. Zhan, Z. Bian, K. Kawabata, M. Ueda, W. Yi, and P. Xue, *Phys. Rev. Lett.* **123**, 230401 (2019).
 - [23] Y. Wu, W. Liu, J. Geng, X. Song, X. Ye, C.-K. Duan, X. Rong, and J. Du, *Science* **364**, 878 (2019).
 - [24] K. Yamamoto, M. Nakagawa, K. Adachi, K. Takasan, M. Ueda, and N. Kawakami, *Phys. Rev. Lett.* **123**, 123601 (2019).
 - [25] M. Naghiloo, N. Abbasi, Y. N. Joglekar, and K. W. Murch, *Nat. Phys.* **15**, 1232 (2019).
 - [26] N. Matsumoto, K. Kawabata, Y. Ashida, S. Furukawa, and M. Ueda, *Phys. Rev. Lett.* **125**, 260601 (2020).
 - [27] C. M. Bender and S. Boettcher, *Phys. Rev. Lett.* **80**, 5243 (1998).
 - [28] C. M. Bender, D. C. Brody, and H. F. Jones, *Phys. Rev. Lett.* **89**, 270401 (2002).
 - [29] C. M. Bender, *Rep. Prog. Phys.* **70**, 947 (2007).
 - [30] A. Mostafazadeh, *J. Math. Phys.* **43**, 205 (2002); *ibid.* **43**, 2814 (2002); *ibid.* **43**, 3944 (2002).
 - [31] A. Mostafazadeh, *Int. J. Geom. Meth. Mod. Phys.* **7**, 1191 (2010).
 - [32] N. Moiseyev, *Non-Hermitian Quantum Mechanics* (Cambridge University Press, Cambridge, UK, 2011).
 - [33] Q.-B. Zeng, Y.-B. Yang, and R. Lü, *Phys. Rev. B* **101**, 125418 (2020).
 - [34] K. Kawabata and M. Sato, *Phys. Rev. Research* **2**, 033391 (2020).
 - [35] Q.-B. Zeng and Rong Lü, *New J. Phys.* **24**, 043023 (2022).
 - [36] S. Yao and Z. Wang, *Phys. Rev. Lett.* **121**, 086803 (2018).
 - [37] S. Yao, F. Song, and Z. Wang, *Phys. Rev. Lett.* **121**, 136802 (2018).
 - [38] V. M. Martinez Alvarez, J. E. Barrios Vargas, and L. E. F. Foa Torres, *Phys. Rev. B* **97**, 121401(R) (2018).
 - [39] V. M. Martinez Alvarez, J. E. Barrios Vargas, M. Berdakin, and L. E. F. Foa Torres, *Eur. Phys. J. Spec. Top.* **227**, 1295 (2018).
 - [40] C. H. Lee and R. Thomale, *Phys. Rev. B* **99**, 201103(R) (2019).
 - [41] H. Zhou and J. Y. Lee, *Phys. Rev. B* **99**, 235112 (2019).
 - [42] K. Kawabata, K. Shiozaki, M. Ueda, and M. Sato, *Phys. Rev. X* **9**, 041015 (2019).
 - [43] N. Okuma and Masatoshi Sato, *Phys. Rev. B* **102**, 014203 (2020).
 - [44] L. Xiao, T. Deng, K. Wang, G. Zhu, Z. Wang, W. Yi, and P. Xue, *Nat. Phys.* **16**, 761 (2020).
 - [45] T. Yoshida, T. Mizoguchi, and Y. Hatsugai, *Phys. Rev. Research* **2**, 022062(R) (2020).
 - [46] S. Longhi, *Phys. Rev. Research* **1**, 023013 (2019).
 - [47] Y. Yi and Z. Yang, *Phys. Rev. Lett.* **125**, 186802 (2020).
 - [48] Q.-B. Zeng and R. Lü, *Phys. Rev. A* **105**, 042211 (2022).
 - [49] Q.-B. Zeng and R. Lü, *Phys. Rev. B* **105**, 245407 (2022).
 - [50] F. K. Kunst, E. Edvardsson, J. C. Budich, and E. J. Bergholtz, *Phys. Rev. Lett.* **121**, 026808 (2018).
 - [51] L. Jin and Z. Song, *Phys. Rev. B* **99**, 081103(R) (2019).
 - [52] K. Yokomizo and S. Murakami, *Phys. Rev. Lett.* **123**, 066404 (2019).
 - [53] L. Herviou, J. H. Bardarson, and N. Regnault, *Phys. Rev. A* **99**, 052118 (2019).
 - [54] Q.-B. Zeng, Y.-B. Yang, and Y. Xu, *Phys. Rev. B* **101**, 020201(R) (2020).
 - [55] D. S. Borgnia, A. J. Kruchkov, and R.-J. Slager, *Phys. Rev. Lett.* **124**, 056802 (2020).
 - [56] Z. Yang, K. Zhang, C. Fang, and J. Hu, *Phys. Rev. Lett.* **125**, 226402 (2020).
 - [57] H.-G. Zirnstein, G. Refael, and B. Rosenow, *Phys. Rev. Lett.* **126**, 216407 (2021).
 - [58] Z. Q. Zhang, H. Liu, H. Liu, H. Jiang, and X. C. Xie, *arXiv:2201.01577*.
 - [59] Y. Xiong, *J. Phys. Commun.* **2**, 035043 (2018).
 - [60] J. C. Budich and E. J. Bergholtz, *Phys. Rev. Lett.* **125**, 180403 (2020).
 - [61] F. Koch and J. C. Budich, *Phys. Rev. Research* **4**, 013113 (2022).
 - [62] N. Hatano and D. R. Nelson, *Phys. Rev. Lett.* **77**, 570

- (1996).
- [63] N. M. Shnerb and D. R. Nelson, *Phys. Rev. Lett.* **80**, 5172 (1998).
- [64] Z. Gong, Y. Ashida, K. Kawabata, K. Takasan, S. Higashikawa, and M. Ueda, *Phys. Rev. X* **8**, 031079 (2018).
- [65] H. Jiang, L.-J. Lang, C. Yang, S.-L. Zhu, and S. Chen, *Phys. Rev. B* **100**, 054301 (2019).
- [66] Q.-B. Zeng and Y. Xu, *Phys. Rev. Research* **2**, 033052 (2020).
- [67] Y. Liu, Y. Wang, X. J. Liu, Q. Zhou, and S. Chen, *Phys. Rev. B* **103**, 014203 (2021).
- [68] Y. Liu, Q. Zhou, and S. Chen, *Phys. Rev. B* **104**, 024201 (2021).
- [69] J. Biddle, D. J. Priour Jr., B. Wang, and S. Das Sarma, *Phys. Rev. B* **83**, 075105 (2011).
- [70] Supplementary material.
- [71] N. Okuma, K. Kawabata, K. Shiozaki, and M. Sato, *Phys. Rev. Lett.* **124**, 086801 (2020).
- [72] K. Zhang, Z. Yang, and C. Fang, *Phys. Rev. Lett.* **125**, 126402 (2020).
- [73] The model Hamiltonian with only t_1 and γ_3 terms is

$$H'_3 = \sum_{j=1}^{L-3} \left[t_1 c_{j+1}^\dagger c_j + t_1 c_j^\dagger c_{j+1} - \gamma_3 c_{j+3}^\dagger c_j + \gamma_3 c_j^\dagger c_{j+3} \right].$$
The model Hamiltonian with only t_1 and γ_4 terms is

$$H'_4 = \sum_{j=1}^{L-4} \left[t_1 c_{j+1}^\dagger c_j + t_1 c_j^\dagger c_{j+1} - \gamma_4 c_{j+4}^\dagger c_j + \gamma_4 c_j^\dagger c_{j+4} \right].$$